A model for "dynamic" roughness in turbulent channel flow

By B. J. McKeon†

A simple model for roughness elements with a time-varying height was used to investigate the effect of time-dependent, "dynamic" roughness on wall-bounded flow. Temporally varying wall velocities were specified in a turbulent channel flow simulation in order to model the effect of introducing a roughness time scale in addition to a distribution of roughness length scales.

1. Introduction

The influence of roughness, specifically the introduction of new length scale(s), on boundary layer flow is a topic of fundamental importance for the understanding and prediction of turbulence structure. It also has important implications for control of skin friction and associated improvements in vehicular efficiency. As such, canonical rough-wall turbulent flows have received a resurgence of interest in recent years (e.g., Jiménez 2004; Flack *et al.* 2005; Gioia & Chakraborty 2006; Allen *et al.* 2007).

The influence of a spatially distributed roughness with a time-varying amplitude has not been explored so extensively. Much previous work on the active control of turbulent wall-bounded flows has focused on the interaction of the flow with discrete actuators, ranging from a single bump rising into a channel flow (Carlson & Lumley 1996) and "active" dimples (McKeon *et al.* 2004), to time-dependent wall motion (Endo & Kasago 2001; Kim *et al.* 2003). However in laminar and transitional flows, White & Saric (2000) investigated the use of pneumatically controlled leading-edge roughness elements to suppress secondary crossflow instabilities and Honsaker & Huebsch (2005) performed a computational study of variable roughness for the control of laminar boundary layer separation from an airfoil.

In this paper we investigate the influence of "dynamic" roughness (where the term "dynamic" implies that a time-dependent amplitude is imposed on geometric perturbations to an otherwise smooth wall such that they move with zero phase velocity) on fully developed turbulent channel flow using a simple model for distributed, time-dependent wall roughness elements implemented in the Direct Numerical Simulation code of Flores & Jiménez (2006).

An ongoing experimental program at the California Institute of Technology seeks to investigate several aspects of "dynamic" roughness in order to diagnose and manipulate the structure of turbulent boundary layers, e.g., a recent APS talk by George *et al.* (2007). The introduction of a roughness time scale via a time-varying roughness amplitude can alternatively be viewed as a structured energy addition at the wall. Forcing specific single frequencies offers the potential for insight into the response of wall-bounded flow to static roughness (in which case the fluctuations at the wall induced by the roughness elements will have a broader frequency spectrum). A further extension of this work is the use

† Graduate Aerospace Laboratories, California Institute of Technology

of this technique as an actuation input for low-effort manipulation and/or control of a receptive flow, i.e., engaging the non-linear nature of the turbulent boundary layer to amplify continuous or "on demand" (on/off) actuation input.

Experimental approaches afford large enough Reynolds numbers for the separation of the characteristic roughness length, denoted here by k_s, viscous and outer scales, i.e., conditions such that both $k_s/\delta \ll 1$ and $k_s^+ = ku_\tau/\nu \gg 1$, leading to a fully rough flow. Here the friction velocity $u_\tau = \sqrt{\tau_w/\rho}$ is defined in terms of the wall shear stress τ_w and the fluid density ρ, and ν is the kinematic viscosity. However the information that can be obtained by interrogation of the flow is (currently) limited to point or planar measurements. In addition, empirical relationships for the skin friction that rely on indirect measurements are not useful unless it is shown that the mean velocity follows the classical smooth wall with a logarithmic profile in the overlap region.

The detailed insight that a parametric study of the influence of the roughness amplitude and frequency would offer, in terms of addressing fundamental scaling questions and extending results from the static roughness parameter space, can be obtained most easily from the full-field information accessible by simulation. However the resolution requirements imposed by the need to resolve the roughness geometry and the smallest turbulent scales, i.e., requiring DNS, alongside scales of the order of one to ten times the outer length scale, suggest that rough-wall flows are difficult to address numerically, at least at high Reynolds numbers. Previous computational investigations of wall turbulence incorporating models for flow over rough walls include an examination of the linearized, time-independent problem using wall-velocity perturbations by Orlandi *et al.* (2003) (where an instantaneous velocity distribution in a plane separating a roughness cavity and the outer flow in a full rough-wall DNS was imposed as the wall boundary condition) and the study of Flores & Jiménez (2006) (in which wall velocities with moments similar to those observed over rough walls were prescribed). Jiménez *et al.* (2001) have also modeled flow over active and passive porous walls using wall velocity disturbances.

We describe here first simulations of a simplified model of dynamically rough walls in turbulent channel flow. There are basic questions to be answered about the resultant structure of the flow, hence significant progress can be made using relatively low Reynolds number channel flow simulations with the appropriate boundary conditions. The main objectives of the proposed research are the development and implementation of a simple model for dynamic roughness, conducive to simulation, in terms of wall velocity disturbances and the formulation of a quantitative description of the subsequent response of mid-Reynolds number turbulent channel flow, identifying the effect of roughness amplitude on the turbulence structure with respect to the smooth-wall case.

2. Approach

2.1. *Direct numerical simulation*

The study was performed using the periodic channel flow DNS code described in Flores & Jiménez (2006), where full details of the numerical methods may be found. In summary, this code solves evolution equations for the wall-normal vorticity, ω_y, and the Laplacian of the wall-normal velocity, $\nabla^2 v$, with pseudospectral spatial discretization. Dealiased Fourier expansions are used in the wall-parallel directions, x and z, and compact finite differences in the wall-normal direction, y. The time integration uses a third-order Runge-Kutta scheme with implicit viscous terms. Flores & Jiménez studied the influence of distributed (temporally constant) wall velocities with zero spatial mean. For this study

FIGURE 1. Schematic of channel and coordinate system.

the code was modified to incorporate spatially distributed, time-dependent wall boundary conditions. The box size was fixed at $3\pi h \times 1.5\pi h$ based on considerations of computational expense; a sketch of the basic geometry and nomenclature used in this study is presented in Fig. 1. An average skin friction was obtained for each run by consideration of the pressure drop along the channel.

While a high Reynolds number is desirable because of the scale separation arguments noted above (at a minimum, a "reasonable" Reynolds number that ensures high Reynolds number wall turbulence characteristics while perhaps not reaching the fully rough condition), a moderate Reynolds number was deemed to be acceptable for this study. Firstly this study represented the first simulation of the problem and secondly high resolution of the spatial distribution of wall velocities with a reasonable run time was preferable. The influence of the boundary condition on the skin friction is not known *a priori*, but a target Reynolds number $Re_\tau = hu_\tau/\nu \sim 500$, where h is the channel half-height, u_τ is the friction velocity and ν is the kinematic viscosity, facilitates future comparison with previous turbulent channel simulations, including the classic smooth-wall case of Kim *et al.* (1987), the 2-D bar roughness of Leonardi *et al.* (2003), the (temporally constant) single wall velocity disturbance approach of Orlandi *et al.* (2003), the Jiménez *et al.* (2001) results for passive and active porous walls (all with $Re_\tau \sim 180$) and the temporally constant wall velocity disturbance study of Flores & Jiménez with $Re_\tau \approx 600$.

2.2. *Dynamic wall boundary condition*

The dynamic wall boundary condition was implemented using a simple model for the roughness elements at both walls, namely linearized boundary conditions for oscillating bumps with simple geometries. The roughness distribution was modeled by replacing the no-slip and impermeability constraints with a temporally harmonic distribution of streamwise and wall-normal velocities at the wall, which can be considered as a crude approximation to boundary conditions corresponding to harmonic dynamic roughness linearized about the turbulent mean velocity profile (note the failure of this approximation for $y < 0$).

In the spirit of Gaster *et al.* (1994), who used this approach to investigate the disturbance field associated with an oscillating bump in a laminar boundary layer (in which, of course, the velocity profile is analytically described for small bump amplitude and continuation can be justified rigorously), we consider turbulent flow with mean velocity distribution $\mathbf{U}(\mathbf{x}, \mathbf{y}, \mathbf{z}) = (U(y), 0, 0)$ over a roughness element with amplitude, $\gamma(x, z, t)$, given by

$$\gamma(x, z, t) = aH(x, z)\cos(\sigma t). \tag{2.1}$$

Here a is the (small) roughness amplitude, $H(x, z)$ is the normalized shape of the rough-

ness elements determined appropriately in order to maintain mass-neutrality and σ is the frequency of the sinusoidal variation of the roughness amplitude. The wall forcing is obtained by writing the velocity near the wall as

$$\vec{u} = \vec{u}_0 + a\vec{u}_1 + a^2\vec{u}_2 + ...,$$

expanding the $\vec{u}_n$ as Taylor series about the wall at $y = 0$ and equating powers of a. Thus

$$u(x,0,z) = -aH(x,z)U'(0)\cos(\sigma t), \quad v(x,0,z) = -\sigma aH(x,z)\sin(\sigma t), \quad w(x,0,z) = 0,$$

where a prime denotes differentiation with respect to y. (Note that generation of zero Reynolds stress at the wall $\overline{uv}_w$ is thus prescribed.) In the absence of *a priori* information on the skin friction, the velocity gradient at the wall, $U'(0)$, was set to the value associated with the smooth-wall run. For a periodic distribution of identical roughness elements with sinusoidal amplitude spatial and temporal variation, the Fourier modes of the wall forcing are given by

$$\tilde{u}_w(k_{x_w}, k_{z_w}) = -a\tilde{H}(k_{x_w}, k_{z_w})U'(0)\cos(\sigma t) \tag{2.2}$$

$$\tilde{v}_w(k_{x_w}, k_{z_w}) = -\sigma a\tilde{H}(k_x, k_z)\sin(\sigma t) \tag{2.3}$$

$$\tilde{w}_w(k_{x_w}, k_{z_w}) = 0, \tag{2.4}$$

and $u = \tilde{u}(y,t)e^{i(k_x x + k_z z)}$, etc. A single wavenumber pair and frequency combination was investigated in this study.

3. Selection of roughness parameters

Selection of dynamic roughness parameters a, k_{x_w}, k_{z_w} and σ from a large parameter space was made by considering the response of flow linearized about the turbulent mean profile to small disturbances in order to ensure a configuration that would elicit a detectable change in the turbulence properties. Since the production of turbulent energy is contained in the linearized equations, it is anticipated that linear analysis gives insight into the receptivity of the flow to specific forcing functions. Linearization about the turbulent mean has been used by Reynolds & Tiederman (1967), among others, to prove linear stability of channel flow. del Álamo & Jiménez (2006) demonstrated that transient growth analysis of the turbulent mean velocity profile combined with the eddy viscosity formulation of Cess (1958) reproduces key features of large- and small-spanwise structures observed in experimental channel flows.

The linear problem may be written for turbulent flow in terms of the modified Orr-Sommerfeld-Squire relationships for wall-normal velocity and vorticity, v and ω_y,where

$$v = \tilde{v}(y,t)e^{i(k_x x + k_z z)}$$

and

$$\omega = \tilde{\omega}(y,t)e^{i(k_x x + k_z z)}$$

using Cess's formulation for the eddy viscosity,

$$\nu_T = \frac{\nu}{2}\left\{1 + \frac{K^2 Re_\tau}{9}[2\eta - \eta^2][3 - 4\eta + \eta^2]^2\left[1 - \exp\left(\frac{-\eta Re_\tau}{A}\right)\right]^2\right\}^{1/2} - \frac{\nu}{2}.$$

Then

$$\frac{\partial}{\partial t}\begin{bmatrix}\tilde{v}\\ \tilde{\omega}_y\end{bmatrix} = \begin{bmatrix}\mathcal{L}_{O-S,mod} & 0\\ \mathcal{L}_c & \mathcal{L}_{SQ,mod}\end{bmatrix}\begin{bmatrix}\tilde{v}\\ \tilde{\omega}_y\end{bmatrix}, \tag{3.1}$$

i.e.,

$$\frac{\partial}{\partial t}\left[\tilde{\mathbf{V}}\right] = \mathcal{L}\left[\tilde{\mathbf{V}}\right], \tag{3.2}$$

with boundary conditions

$$\tilde{v} = \frac{\partial \tilde{v}}{\partial y} = \tilde{\omega} = 0 \quad \text{when} \quad y = 0, 2.$$

Here the coupling operator, $\mathcal{L}_c$, has the same form as in the laminar base flow case

$$\mathcal{L}_c = -iU'k_z \tag{3.3}$$

and the modified Orr-Sommerfeld and Squire operators, $\mathcal{L}_{O-S,mod}$ and $\mathcal{L}_{SQ,mod}$, respectively, are given as follows

$$\mathcal{L}_{O-S,mod} = (\mathcal{D}^2 - k^2)^{-1}(-i)\left[-k_xU'' + k_xU(\mathcal{D}^2 - k^2) + i(\mathcal{D}^2 - k^2)(E - \nu_T k^2) - iB\right] \tag{3.4}$$

$$\mathcal{L}_{SQ,mod} = (-i)[k_xU + (E - k^2\nu_T)i], \tag{3.5}$$

with

$$E = \frac{\partial}{\partial y}\left(\nu_T\frac{\partial}{\partial y}\right),$$

$$B = \frac{\partial}{\partial y}\left(\frac{\partial}{\partial y}\left[\frac{\partial \nu_T}{\partial y}\frac{\partial}{\partial y}\right]\right),$$

$\mathcal{D}^2 = \frac{\partial^2}{\partial y^2}$ and $k^2 = k_x^2 + k_z^2$.

The expression given in Eq. 3.1 can be formulated in terms of the resolvent by considering perturbations $\mathbf{f}$ to the linearized Navier-Stokes equations of Eq. 3.2 for $\tilde{v}$ and $\tilde{\omega}$ that vary harmonically with frequency σ, i.e.,

$$\tilde{\mathbf{V}} = (i\sigma\mathcal{I} - \mathcal{L})^{-1}\left[\tilde{\mathbf{f}}\right],$$

where $\mathcal{I}$ is the identity matrix. A Singular Value Decomposition (SVD) of the discrete resolvent, $\mathcal{R} = (i\sigma\mathcal{I} - \mathcal{L})^{-1}$ ranks the forcing and response pairs in terms of the energy norm, where the (algebraic) growth of input disturbances arises due to the non-normality of the linear operator. The first singular value, here denoted A_1, is associated with the mode pair that experiences the most energy amplification (this is a linear amplification mechanism that occurs despite the linear stability of the turbulent mean velocity profile): it is assumed that a wall forcing which can introduce a disturbance that resembles/excites this forcing mode would result in a response mode with a significant amplitude. Note that this is not the mode with a global maximum in amplification associated with zero streamwise wavenumber, nor the result of the initial condition problem examined in del Álamo & Jiménez (2006).

Figure 2 shows the variation of the maximum singular value, A_1, with (k_z, σ) for a fixed $k_x = 2$ dictated by the box size, namely requiring at least three roughness wavelengths in the x-direction, for $Re_\tau = 500$. A local maximum occurs for $k_z = 4$ and $\sigma = 1.45$; the corresponding forcing and response modes are shown in Fig. 3. It can be seen that these are wall modes, so it is realistic to assume that wall forcing could excite a similar type of perturbation. The dominant forcing and largest growth in the wall-parallel velocity

Case	Re_τ	L_x/h	L_z/h	a^+	u'^+_w	v'^+_w	w'^+_w	$k_{x_w}h$	$k_{z_w}h$
1	495	3π	1.5π	–	–	–	–	–	–
2	491	3π	1.5π	5	3.53	0.21	0	2	4
3	485	3π	1.5π	10	7.07	0.41	0	2	4

TABLE 1. Summary of run conditions.

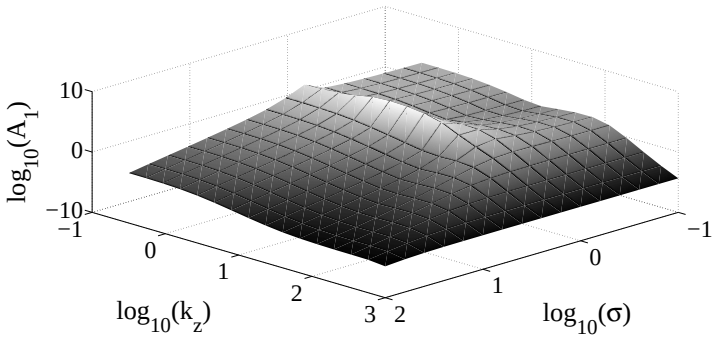

FIGURE 2. Variation of the leading singular value, A_1, with k_z and σ for prescribed parameters $k_x = 2$ and $Re_\tau = 500$.

components reflects the amplification of the wall-normal vorticity at the expense of the wall-normal velocity.

We consider the linear addition of upstream- and downstream-moving forcing modes with the same wavenumbers and frequency in order to generate a standing wave at the wall, where in a linear sense the former is damped and, as just demonstrated, the latter is amplified. A summary of the run conditions is presented in Table 1. Three different roughness amplitudes, $a^+ = 0, 5, 10$, were considered. The magnitude of at least the last roughness amplitude suggests that these disturbances would be out of the linear regime so that the above analysis is not strictly valid, however it is used as a guide for the selection of the roughness parameters.

4. Results and discussion

4.1. *Velocity statistics*

Consider first the smooth-wall case. The first and second moments of the streamwise velocity for the smooth-wall case, $a^+ = 0$, are shown in inner scaling in Figs. 4 and 5. At this relatively low turbulent Reynolds number, there is about half a decade of at least approximate logarithmic scaling in the smooth-wall mean velocity, depending on the definition of the limits of the log law. The near-wall peak in turbulence intensity centered at $y^+ \approx 15$ is also observed.

A roughness amplitude of $a^+ = 5$ has negligible effect on the mean velocity but leads to a considerable increase in turbulent fluctuation energy close to the wall (Figs. 4 and 5). The increase in the streamwise and wall-normal components, u'^+ and v'^+, where

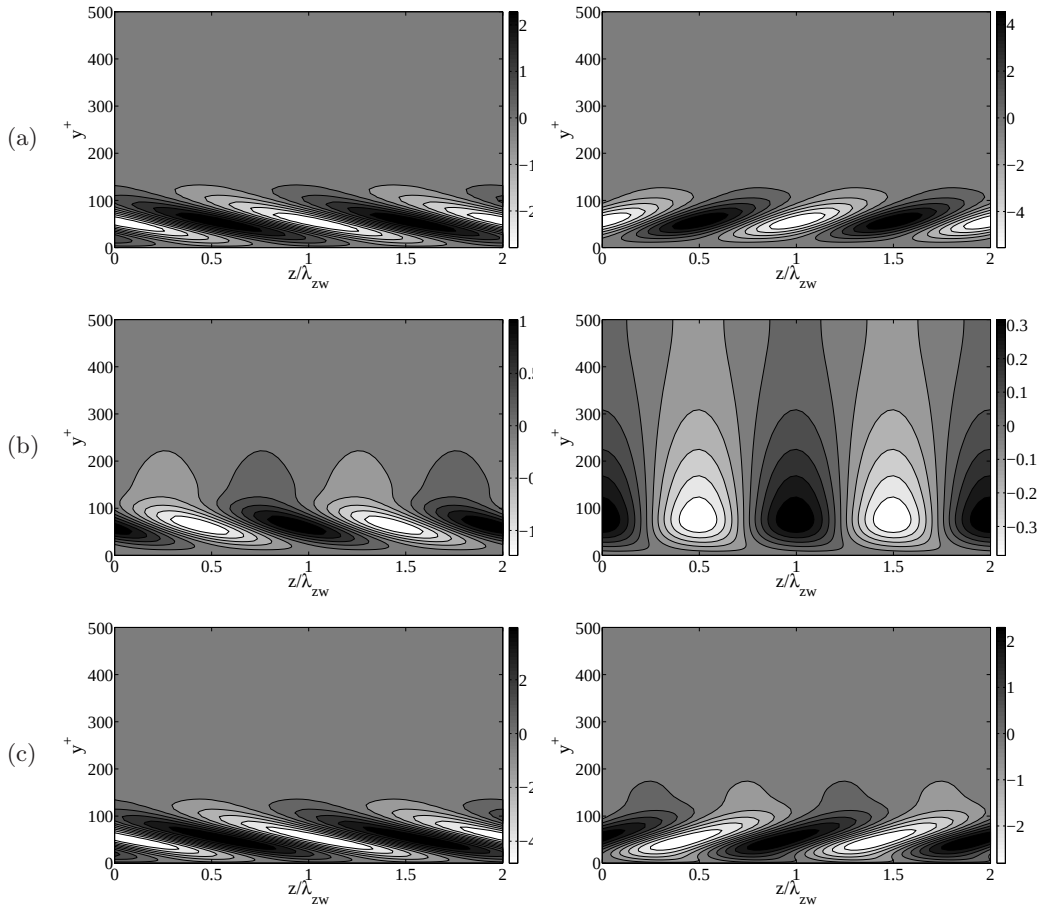

FIGURE 3. Forcing (left) and response (right) modes corresponding to the local maximum in A_1 indicated in Fig. 2 at $k_x = 2$, $k_z = 4$ and $\sigma = 1.45$ and $Re_\tau = 500$. (a) Streamwise velocity, u; (b) spanwise velocity, w; (c) wall-normal velocity, w.

$u_i' = \sqrt{\overline{u_i^2}}$, is confined to y^+ values below the near-wall turbulence peak, while the spanwise component, w'^+, is essentially unaffected by the roughness. The larger influence on u'^+ reflects the dominance of the u forcing term in the dynamic roughness model for this particular combination of roughness parameters. Note that no consideration is made of a roughness-induced offset in the origin.

When the roughness amplitude is increased to $a^+ = 10$, a skin friction reduction of $\sim 5\%$ is obtained, corresponding to a Hama roughness function, $\Delta U^+ = -0.4$. The roughness-induced perturbations persist further from the wall in all three components, notably exciting the spanwise component in this case. Even at the larger roughness amplitude the outer flow appears to obey Townsend's similarity hypothesis, with collapse of the profiles in outer scaling (not shown).

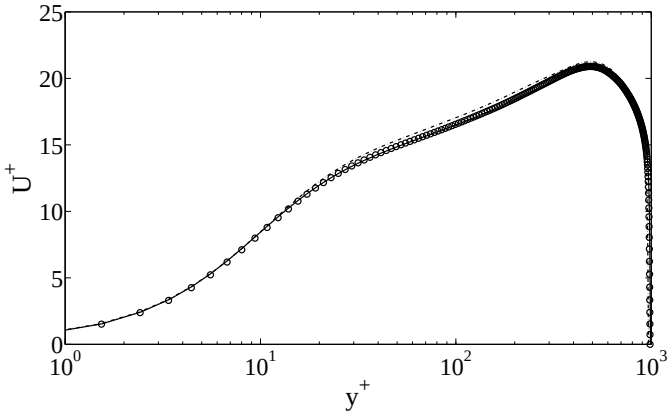

FIGURE 4. Variation of the mean velocity profile with wall-normal distance in inner scaling. ——— : $a^+ = 0$, $\circ\circ\circ$: $a^+ = 5$ and $- \cdot - \cdot -$: $a^+ = 10$.

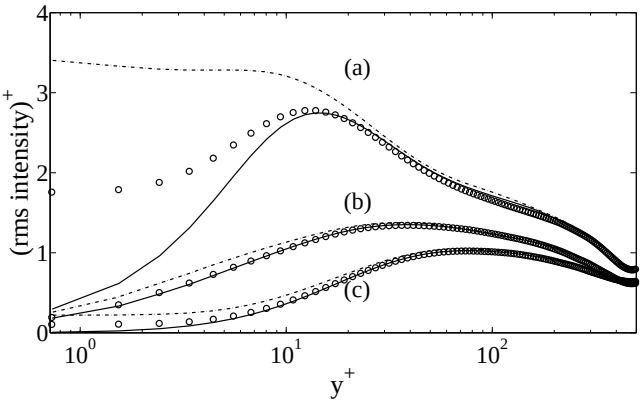

FIGURE 5. Root-mean-square energy of the inner-scaled turbulent fluctuations, (a) u'^+, (b) w'^+ and (c) v'^+. ——— : $a^+ = 0$, $\circ\circ\circ$: $a^+ = 5$ and $- \cdot - \cdot -$: $a^+ = 10$.

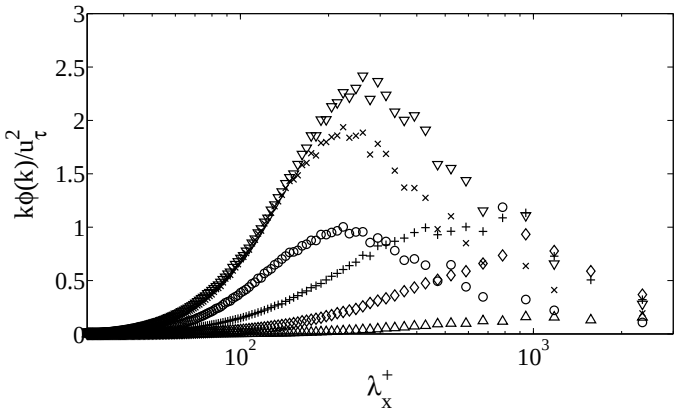

FIGURE 6. Variation of the premultiplied power spectra with wavenumber for the $a^+ = 0$, smooth-wall case. $\circ$: $y^+ = 4$; $\times$: $y^+ = 8$; ∇: $y^+ = 20$; $+$: $y^+ = 60$;$\diamond$: $y^+ = 128$; $\triangle$: $y^+ = 500$.

4.2. *Power spectra*

Consideration of the variation of the form of the streamwise velocity spectra with wall-normal distance helps to illuminate the mechanism by which the roughness influences the near-wall flow. Figure 6 shows the development of the premultiplied spectra with y^+ for the smooth-wall case. The log scale on the abscissa means that equal area beneath the spectra corresponds to equal energy. These spectra can be assembled into a composite contour plot by interpolating between data at different wall-normal locations, in the form of the top panel of Fig. 7. The center and bottom panels show the corresponding plots for $a^+ = 5$ and 10, respectively. An energy peak at a high wavelength corresponding to the forcing wavelength of u_w can be clearly seen for the dynamically rough wall flows. For $a^+ = 10$, additional energy resides at half the forcing wavelength. Further investigation of the structure leading to an induced spanwise component may provide additional information. The introduction of energy at a shorter wavelength than the forcing could suggest an analogy with the introduction of a streamwise asymmetry in the fluctuations close to the wall induced by the roughness elements associated with separation from the bump surfaces in the real case. Note that this wavelength ($\lambda_x \approx 800$) also suggests a potential interaction with the existing streak pattern associated with the near-wall cycle.

It is hypothesized that the emergence of this second spectral peak correlates with the observance of the reduction in skin friction. Consideration of the fluctuating streamwise vorticity, ω'_x, in Fig. 8 shows that increasing the amplitude of the dynamic roughness increases the magnitude of the vorticity near the wall. The relationship between the forcing and the smooth-wall near-wall turbulence production cycle remains to be determined, as does any connection to the influence of spanwise oscillations on turbulent flow, e.g., Mangiavacchi & Akhavan (1992). Note that for $a^+ = 10$ only, w'^+ in the near-wall region is increased above the smooth-wall value.

5. Conclusions

Direct numerical simulations of turbulent channel flow with a simple model for a dynamically rough wall with two different amplitudes of roughness were compared to the smooth-wall case. Significant roughness amplitudes were required in order to cause any change to the first and second moments beyond a local Stokes' layer dictated by the imposed wall velocity disturbances. When $a^+ = 10$, a small reduction in skin friction was obtained; however this is likely a low Reynolds number control mechanism.

The roughness model is a crude one, and the linear assumption is not valid for the roughness considered here. However, useful insights into the effect of wall forcing on the near-wall turbulence were obtained. Further work will be required to investigate changes to the turbulence structure induced by dynamic roughness elements of different geometries in low and high Reynolds number flows and to compare the result of this work to known passive control strategies, such as spanwise wall oscillation and regularization of the near-wall flow.

Acknowledgements

The author wishes to thank Javier Jiménez for generously permitting the use of the DNS code and for useful conversations and ideas, and Sanjeeb Bose for computational support during the program.

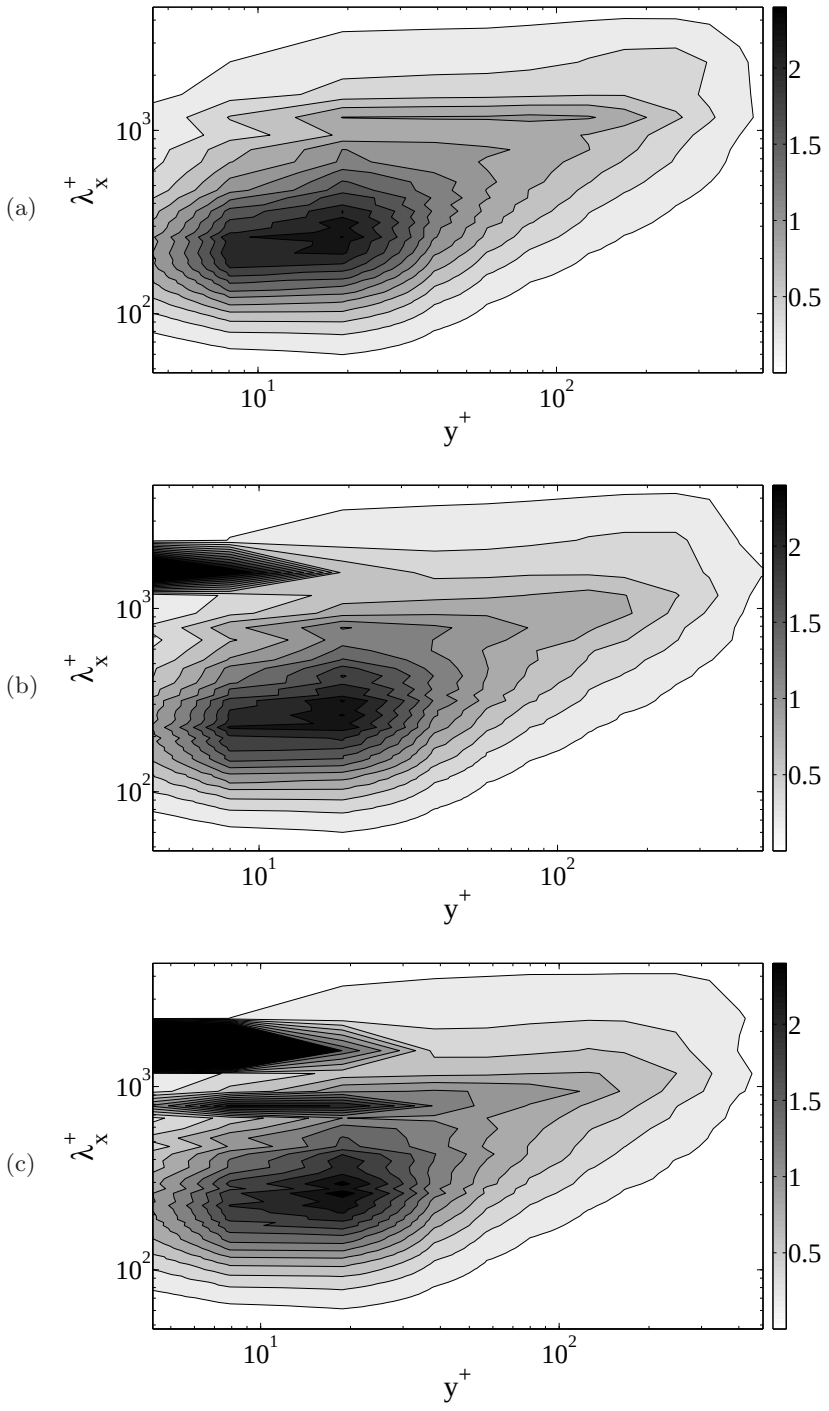

FIGURE 7. Composite spectrograms showing the variation of the premultiplied spectrum, $k\phi(k)/u_\tau^2 = kh\phi(kh)/u_\tau^2$, with wall-normal distance. (a) $a^+ = 0$, (b) $a^+ = 5$ and (c) $a^+ = 10$.

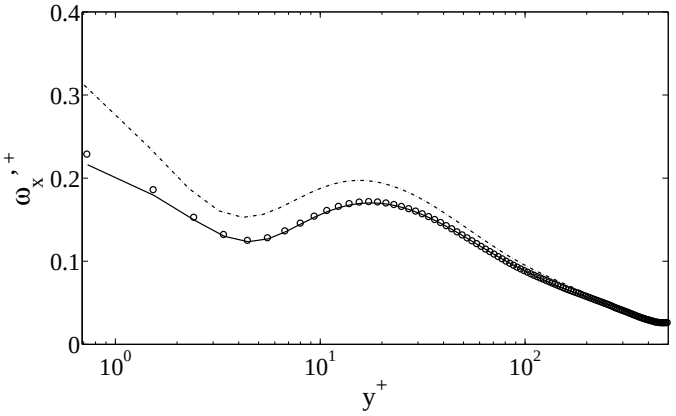

FIGURE 8. Wall-normal profiles of the root mean squared (fluctuating), streamwise vorticity. ——— : $a^+ = 0$, ○ ○ ○ : $a^+ = 5$ and $- \cdot - \cdot -$: $a^+ = 10$.

REFERENCES

DEL ÁLAMO, J. C. & JIMÉNEZ, J. 2006 Linear energy amplification in turbulent channels. *J. Fluid Mech.* **559**, 205–213.

ALLEN, J. J., SHOCKLING, M. A., KUNKEL, G. J. & SMITS, A. J. 2007 Turbulent flow in smooth and rough pipes. *Phil. Trans. R. Soc. A* **365**, 699–714.

CARLSON, A. & LUMLEY, J. L. 1996 Flow over an obstacle emerging from the wall of a channel. *AIAA Journal* **34** (5), 924–931.

CESS, R. D. 1958 A study of the literature on heat transfer in turbulent tube flow. *Tech. Rep.* Rep. 8-0529-R24. Westinghouse Research, Pittsburgh, PA.

ENDO, T. & KASAGI, N. 2001 Active control of wall turbulence with wall deformation. *JSME Int. J., Series B* **44** (2), 195–203.

FLACK, K. A., SCHULTZ, M. P. & SHAPIRO, T. 2005 Experimental support for Townsend's Reynolds number similarity hypothesis on rough walls. *Phys. Fluids* **17** (035102).

FLORES, O. & JIMÉNEZ, J. 2006 Effect of wall-boundary disturbances on turbulent channel flows. *J. Fluid Mech.* **566**, 357–376.

GASTER, M., GROSCH, C. E. & JACKSON, T. L. 1994 The velocity field created by a shallow bump in a boundary layer. *Phys. Fluids* **6** (9), 3079–3085.

GEORGE, J., LEHEW, J. & MCKEON, B. J. 2007 The response of turbulent boundary layers to dynamic roughness perturbations. *Bulletin of the American Physical Society* **52** (17).

GIOIA, G. & CHAKRABORTY, P. 2006 Turbulent friction in rough pipes and the energy spectrum of the phenomenological theory. *Phys. Rev. Lett.* **96** (044 502).

HONSAKER, R. & HUEBSCH, W.W. 2005 Parametric study of dynamic roughness as a mechanism for flow control. *AIAA 2005-4732*.

JIMÉNEZ, J. 2004 Turbulent flows over rough walls. *Annu. Rev. Fluid Mech.* **36**, 173–196.

JIMÉNEZ, J., UHLMANN, M., PINELLI, A. & KAWAHURA, G. 2001 Turbulent shear flow over active and passive porous surfaces. *J. Fluid Mech.* **442**, 89–117.

KIM, C., JEON, W.-P., PARK, J. & CHOI, H. 2003 Effect of a localized time-periodic wall motion on a turbulent boundary layer flow. *Phys. Fluids* **15** (1), 265–268.

Kim, J., Moin, P. & Moser, R. 1987 Turbulence statistics in fully developed channel flow at low Reynolds number. *J. Fluid Mech.* **177**, 133–166.

Leonardi, S., Orlandi, P., Smalley, R. J., Djenidi, L. & Antonia, R. A. 2003 Direct numerical simulations of turbulent channel flow with transverse square bars on one wall. *J. Fluid Mech.* **491**, 229–238.

Mangiavacchi, W. J. J. N. & Akhavan, R. 1992 Suppression of turbulence in wall-bounded flows by high-frequency spanwise oscillations. *Phys. Fluids A* **4**, 1605–1607.

McKeon, B. J., Lambert, S., Sherwin, S. J. & Morrison, J. F. 2004 Active dimples for flow control. In *Proc. 10th European Turbulence Conference*. CIMNE.

Orlandi, P., Leonardi, S., Tuzi, R. & Antonia, R. A. 2003 Direct numerical simulation of turbulent channel flow with wall velocity disturbances. *Phys. Fluids* **15** (12), 3587–3601.

Reynolds, W. C. & Tiederman, W. G. 1967 Stability of turbulent channel flow, with application to Malkus's theory. *J. Fluid Mech.* **27**, 253–272.

White, E. B. & Saric, W. S. 2000 Application of variable leading-edge roughness for transition control on swept wings. *AIAA 2000-0283*.